arXiv:cond-mat/0609148v1 [cond-mat.mes-hall] 6 Sep 2006

Effect of free carriers and impurities on density of states and optical spectra of two-dimensional magneto-excitons

Anna Gładysiewicz, Leszek Bryja, and Arkadiusz Wójs
Institute of Physics, Wrocław University of Technology, Wybrzeże Wyspiańskiego 27, 50-370 Wroclaw, Poland

Marek Potemski
Grenoble High Magnetic Field Laboratory, CNRS, F-38042 Grenoble Cedex 9, France

Density of states (DOS) and absorption spectrum of weakly doped, narrow quantum wells in high magnetic fields are calculated by realistic exact diagonalization. The systems containing an electron–hole pair with and without an additional, second electron are compared. In DOS, the exciton–electron interaction is shown to fill the gaps between Landau levels and to yield additional discrete peaks corresponding to bound trion states. In absorption, interaction with the additional free electron causes no shift or renormalization of main, excitonic peaks. However, it results in additional, weaker peaks associated with bound trions in the lowest or higher Landau levels. The calculation is supplemented with experimental photoluminescence and photoluminescence-excitation studies of two-dimensional holes and electrons in high magnetic fields.

PACS numbers: 71.35.Pq, 71.35.Ji, 71.10.Pm

I. INTRODUCTION

Trions (also called charged excitons) are bound states of a neutral exciton (electron–hole pair, $X = e + h$) with an additional carrier, either electron or valence hole, for a negative ($X^- = 2e + h$) or positive trion ($X^+ = 2h + e$), respectively.[1,2] Neutral and charged excitons occur naturally in photoluminescence (PL) experiments, in which creation or annihilation of e–h pairs accompanies interband absorption or emission of light.[3] While excitons are expected in charge-neutral systems, formation of trions depends on the presence of free carriers.

The trion binding energy Δ is defined as the effective attraction between an exciton and an additional carrier ($\Delta = E[X] + E[e] - E[X^{\pm}]$, where $E[\ldots]$ is the ground energy of a given complex). An important material parameter affecting Δ is the ratio of electron and hole effective masses,[4] $\eta = \mu_e/\mu_h$; for $\eta = 0$ the X^- dynamics reduces to a familiar problem of the D^- center.[5,6] Originating from charge-dipole interaction, trion binding is usually much weaker than the exciton binding. However, its strong enhancement by spatial confinement and/or magnetic field B was predicted.[7] The pioneering experiment of Kheng *et al.*[2] in CdTe, followed by a series of measurements in GaAs[8,9,10,11] and ZnSe[12,13] confirmed that it is sufficient for the trion's detection. The X^+ was also observed[14,15] and shown to be different from X^- (due to the $\eta \leftrightarrow \eta^{-1}$ asymmetry).

In a typical experimental configuration, a quantum well containing a quasi-two-dimensional (2D) electron (or hole) gas is placed in the perpendicular field. The field should be sufficiently strong to induce magnetic quantization of single-particle states into macroscopically degenerate Landau levels (LLs), with the inter-LL (cyclotron) spacing $\hbar\omega_c$ which is at least comparable to the effective excitonic Rydberg ($Ry \approx 5.5$ meV in GaAs). The well width w should not be much greater than the effective excitonic Bohr radius ($a_B \approx 10$ nm in GaAs) and the magnetic length ($\lambda = \sqrt{hc/eB} \approx 8.1$ nm at $B = 10$ T).

The quantum-mechanical problem of a 2D exciton in a high magnetic field goes back several decades.[16,17,18] The continuous (owing to the neutral charge) energy dispersion in some idealized situations is known analytically, and the deviations due to inter-LL mixing or finite well width have been studied experimentally and numerically.[19] The simple $q = 0$ optical selection rule (q being the wavevector of an annihilated e–h pair) results from the small momentum carried by the absorbed/emitted photon. In experiment, the excitonic recombination is usually observed in PL of quantum wells containing no free carriers.

2D trions at high B have also been extensively studied in the past.[20] Different theoretical/computational approaches and the key results have been discussed in an exhaustive review by Peeters, Riva, and Varga.[21] Depending on the parameters (e.g., w and B), the trion energy spectrum contains one or more bound states, which can be conveniently labeled by total spin S of the pair of electrons and total angular momentum M. At small B, the only bound X^- state is the spin-singlet with $S = 0$ and $M = 0$, equivalent to a 2D Hydrogen ion.[2,8,9,10,11] In the (unrealistic) limit of very high B and vanishing w, the singlet unbinds, and it is replaced by the spin-triplet with $S = 1$ and $M = -1$.[22,23] A triplet trion was identified by Shields *et al.*[10] (although now it is not clear if it was the $M = -1$ triplet ground state). The singlet–triplet crossover was predicted[24] in rather high fields (e.g. $B \approx 30$ T in narrow symmetric GaAs wells). Despite initial difficulties[25] it was also eventually confirmed in several experiments.[26,27,28,29] Additional bound states were predicted[30] at intermediate B, but (for realistic parameters) they are always less strongly bound than the above two. These states were also confirmed by both independent calculations[31] and by experiments.[27,28,32]

The pair of optical selection rules results from invariance under (magnetic) translations[33,34] and from the particle–hole symmetry between conduction electrons and valence holes.[35,36,37] Both these "geometric" and "hidden" symmetries are at least weakly broken in realistic conditions. Nevertheless, recombination of trions with $M \neq 0$ requires a symmetry-breaking collision (with an impurity or another carrier), and therefore, it became customary to label different trions as "bright" and "dark" (meaning having $M = 0$ and $M \neq 0$, respectively). In most recent experiments,[25,27,32] up to three trion states are observed: "bright" singlet $X_{\rm s}^-$, "dark" triplet $X_{\rm td}^-$, and a weakly bound "bright" triplet $X_{\rm tb}^-$ with $S = 1$ and $M = 0$. Vanishing oscillator strength,[23,34] of $X_{\rm td}^-$ confirmed directly in optical absorption,[38] makes it more difficult to observe (even in PL) than the other trions. In fact, this state had not been conclusively identified until the work of Yusa *et al.*,[27] motivated by earlier high-field experiments (especially of Hayne *et al.*,[25] showing apparent discrepancy with prediction[24] of singlet–triplet crossing, but also several others[26] showing inconsistent features in trion spectra) and a numerical prediction[30] of an excited triplet state, $X_{\rm tb}^-$. Most recently, additional weakly bound states were reported[29] in CdTe ($Ry \sim 10$ meV, about twice larger than in GaAs).

Involving only three particles, trion's quantum dynamics might appear to be relatively simple, both conceptually and computationally. Addition of high magnetic field and confinement does not add much complexity, and indeed, quantum numbers and symmetries of all bound trions (in wide range of realistic conditions) are by now understood. In short, the dynamics depends on competition of several energy scales, with the following characteristic values for our example of a 15 nm symmetric GaAs well at $B = 10$ T: cyclotron gap ($\hbar\omega_c \sim 18$ meV for electrons and ~ 4 meV for heavy holes), Coulomb energy ($e^2/\lambda \sim 14$ meV), and a small Zeeman gap. The well width w comes in two places, defining excitation gaps to higher subbands (gap to the second subband is ~ 50 meV for electrons and ~ 10 meV for the holes) and affecting in-plane Coulomb matrix elements (this effect is parametrized by $w/\lambda \sim 2$). Also, even weak asymmetry between electron and hole subband wavefunctions $\chi_s(z)$ can considerably affect the trion binding, since it leads to different magnitudes of e–e and e–h interactions, which no longer cancel in Δ (this effect is essential in asymmetric wells, not considered here, where the asymmetry depends on carrier concentration and/or additional gates).

However, the above optimistic (and popular) view hides the fact that good understanding of the role of trions in PL experiments must include variety of complications due to coupling to the environment (e.g., complex single-particle energy band structure with nonparabolic and anisotropic dispersions, interaction with free carriers, lattice defects, and phonons, spin-orbit effects, etc.). Some quantities (e.g., the binding energies, especially of the triplet states) can be calculated rather accurately.[30,31] However, others (such as the critical values of B and w for the singlet–triplet transitions) depend so sensitively on the (often unknown) parameters that their quantitative modeling turns out somewhat pointless. Another unsolved (quantitatively) and important problem is the kinetics of trions,[39,40] involving their binding/unbinding ($X^- \leftrightarrow X + e^-$) and, at high B, orbital/spin relaxation ($X_{\rm s}^- \leftrightarrow X_{\rm td}^- \leftrightarrow X_{\rm tb}^-$).

In this article, we analyze the effect of trions on the optical absorption spectrum of 2D electrons in a magnetic field. Thus, in addition to the earlier studied bound trion states,[30,31] the entire low-energy $2e + h$ spectrum is considered. In a somewhat related work, asymmetry of trion absorption peaks at small B was discussed by Stebe *et al.*[41] The inclusion of only two electrons and one hole in the model restricts it to the "dilute" regime, defined by a small value of the filling factor, $\nu \ll 1$ (ν is defined as the number of electrons N divided by the LL degeneracy g; alternatively, $\nu = 2\pi\varrho\lambda^2$ where ϱ is the 2D electron concentration). It is remarkable that in some systems the immersed trion is only weakly (perturbatively) affected by the surrounding electrons. In narrow wells and in high magnetic fields, this occurs at $\nu < \frac{1}{3}$ due to "Laughlin correlations"[42] between electrons and trions,[43] preventing strong e–X^- collisions (indeed, in wider wells trions seem to be strongly coupled to the electrons and cannot be regarded as simple three-body quasiparticles[44]).

The density of states (DOS) and absorption spectra are calculated numerically by exact diagonalization in Haldane's spherical geometry.[45,46] The figures were drawn for a particular choice of a symmetric $w = 15$ nm GaAs quantum well at $B = 10$ T. Since absorption into bound trion states was studied earlier, we concentrate on the effects of the interaction of the exciton with a (single) *unbound* electron. The main conclusions are redistribution of the density of states (by filling the gaps between the LLs) and the emergence of additional, trion peaks in the absorption spectrum (also in the excited LLs).

The calculation is supplemented with the results of experimental polarization-resolved photoluminescence (PL) and photoluminescence-excitation (PLE) studies of a 2D hole and electron gases in a symmetric 15 nm GaAs well. Presented spectra reveal absorption into a pair of bright trions in the lowest LL and emission from these two states, the exciton, and the dark triplet trion.

II. MODEL

The $e + h$ and $2e + h$ energy spectra are calculated by exact diagonalization of the hamiltonian matrix on a Haldane sphere, convenient for modeling an infinite plane with 2D translational invariance. In this geometry, the magnetic field normal to the spherical surface of radius R is produced by a Dirac monopole od strength $2Q = 4\pi R^2/\phi_0$ ($\phi_0 = hc/e$ is the magnetic flux quantum). Through the following relation, $R^2 = Q\lambda^2$, monopole strength determines surface curvature (in the magnetic units).

The single-particle states are called monopole harmonics.[45] They are the eigenstates of angular momentum l and its projection m on the z-axis. The lowest shell, corresponding to the lowest LL, has $l = Q$ and finite degeneracy $g = 2Q+1$. Higher shells, corresponding to the excited LLs labeled by index n, have $l = Q + n$.

The energy of the nth shell is $\varepsilon_n = \hbar\omega_c(n + \frac{1}{2}) + \hbar^2 n(n+1)/2\mu R^2$. It contains the cyclotron gap (with $\omega_c = eB/\mu c$, where μ is the effective mass) and an additional, curvature-dependent term. In order to model a real structure, we take advantage of the LL structure of monopole harmonics, but replace ε_n with the correct energies of electron and hole LLs. E.g., at $B = 10$ T, we use $\hbar\omega_c = 17.8$ meV for electrons and 3.7 meV for the heavy hole (the latter value taken after Cole *et al.*[47] for $w = 15$ nm).

The second-quantization hamiltonian reads

$$H = \sum_i c_i^\dagger c_i \varepsilon_i + \sum_{ijkl} c_i^\dagger c_j^\dagger c_k c_l v_{ijkl}. \qquad (1)$$

An additional term $\sum_{ij} c_i^\dagger c_j u_{ij}$ will also be included to describe interaction with a positive or negative point charge. Here, $c_i^\dagger$ and c_i are operators creating and annihilating a conduction electron or a valence hole, in the state labeled by a composite index i containing all relevant single-particle quantum numbers (band β, subband s, LL index n, angular momentum m, and spin σ).

The Coulomb interaction matrix elements v and u in the basis of monopole harmonics are known analytically for all particles confined to a 2D surface of the sphere. However, to account for a finite width of the real quantum well, we have integrated all matrix elements numerically, in 3D, using form-factors appropriate for the actual electron and hole subband wavefunctions $\chi_s(z)$. Mixing with higher quantum well subbands (excited states in the z-direction, labeled by $s > 0$) is not very strong in a narrow and symmetric well due to high quantization energy (for $w = 15$ nm and $Al_0.35Ga_{0.65}As$ barriers, it is 49.1 meV and 11.5 meV to the first excited electron and hole subbands, respectively; calculation after Ref. 48) and the parity conservation. Nevertheless, it is not quite negligible for the bound states (states with strong interactions).

Without impurities, the $e + h$ and $2e + h$ eigenstates of H are labeled by total angular momentum L and its projection L_z. When converting these quantities to the planar geometry, neutral and charged states must be treated differently: L of an e–h pair represents wavevector $q = L/R$, and for a $2e + h$ state it corresponds to $M = L - Q$. The $2e + h$ eigenstates are also labeled by spin S of the pair of electrons and its projection S_z. The calculation need only be performed in the $L_z = S_z = 0$ subspace and the appropriate Zeeman shift can be added at the end to the energies of each triplet ($S = 1$) state.

With an impurity placed at a north pole of the sphere, L_z is still conserved, but L is not. Only the $S_z = 0$ subspace need be considered, but a separate diagonalization must be performed for each L_z.

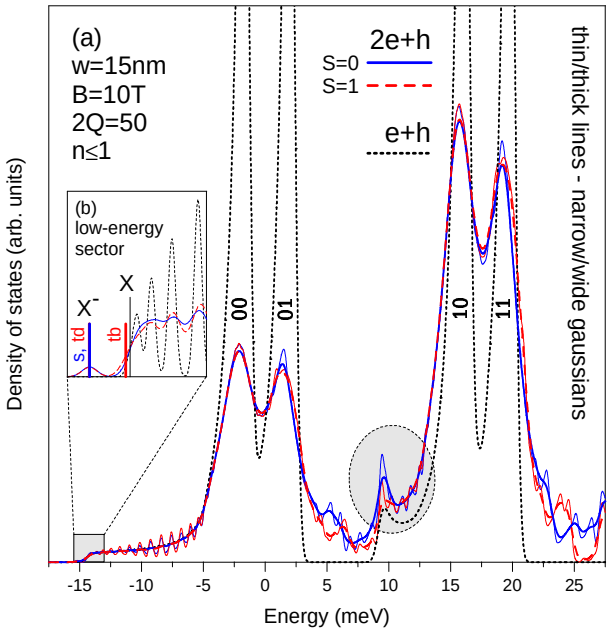

FIG. 1: (color online) Density of states (DOS) of $e + h$ and $2e + h$ systems in a symmetric GaAs quantum well of width $w = 15$ nm at magnetic field $B = 10$ T, calculated on Haldane sphere with a large magnetic monopole strength $2Q = 50$ including only two lowest electron and hole LLs ($n \le 1$). Continuous curves were obtained from finite-size discrete energy spectra by gaussian broadening. For $2e+h$, DOS is divided by $g = 2Q+1$ (LL degeneracy of the second electron), and singlet and triplet configurations (spin $S = 0$ and 1) are drawn separately. For $e+h$, LL indices "$n_e n_h$" mark the strongest peaks. Inset: magnified lowest-energy sector (vertical lines mark position of discrete bound trions and the excitonic ground state.

The $2e + h$ diagonalization was carried out in configuration-interaction basis, $|i, j; k\rangle = c_i^\dagger c_j^\dagger c_k^\dagger |\text{vac}\rangle$. Here indices i and j denote the occupied electron states, k describes the hole, and $|\text{vac}\rangle$ is the vacuum state. Similarly, the basis for the $e + h$ calculation was $|i; k\rangle$. As mentioned earlier, only the spin-unpolarized states with $L_z \equiv m_i + m_j - m_k = 0$ are included in the basis. To find eigenstates corresponding to given (L, S) we used a modified Lanczos algorithm, with additional projection of Lanczos vectors at each iteration.

III. RESULTS AND DISCUSSION

A. Density of States

We begin by the calculation of the density of states DOS $= d\Gamma/dE$ (the number of states Γ per unit of energy E). In Fig. 1 we compare the results for $e + h$ and $2e + h$ obtained for a rather large $2Q = 50$ and including only the lowest two electron and hole LLs ($n \le 1$). The discrete energy spectra obtained from finite-size calculation were converted to the continuous lines shown in the

figure by broadening with Gaussians,

$$\mathrm{DOS}(E) = \sum_i \mathcal{G}_\delta(E - E_i), \qquad (2)$$

where the summation goes over all energy levels E_i and $\mathcal{G}_\delta(x) = \delta^{-1}\pi^{-1/2}\exp(-x^2/\delta^2)$. Thin and thick lines correspond to two different broadening widths $\delta = 0.2$ and 0.5 meV. Blue solid, red dashed, and black dotted lines were used to distinguish $2e+h$ ($S = 0$ and 1 plotted separately; only $S_z = 0$ is shown for $S = 1$) from $e+h$. To compare DOS for $e+h$ and $2e+h$, the latter curve was rescaled from the value defined by Eq. (2) by $g^{-1} = (2Q+1)^{-1}$ (i.e., divided by the number of states available to the second electron). Energy E is measured from the noninteracting configurations in the lowest LL.

For a noninteracting e–h pair, DOS consists of discrete peaks labeled by the LL indices for both particles, "$n_e n_h$". The black dotted curve demonstrate the effect of e–h interaction. Within each pair of LLs, magneto-excitonic dispersion becomes flat at long wavevectors q, corresponding to the vanishing e–h attraction. Therefore, although smeared toward lower energies, strong "$n_e n_h$" peaks persist. In our calculation, restricted area of the sphere prohibits the pair to separate in the $q \to \infty$ limit (the range of $q = L/R$ is restricted by $L \le 2Q$), and the "$n_e n_h$" peaks have finite height and are displaced to the left by the remnant attraction ($\sim e^2/2R = (2\sqrt{Q})^{-1}\, e^2/\lambda$). This redshift ($\sim 1.4$ meV for $2Q = 50$) is a finite-size artifact. The low-energy tail extends from each "$n_e n_h$" peak over the range of the excitonic binding energy within the corresponding pair of LLs. Since e^2/λ is larger than $\hbar\omega_c$ of the holes, these tails essentially close the gaps between the neighboring hole LLs. Thin lines (shown in the magnified low-energy sector in the inset) reveal artificial size quantization on a sphere ($L = 0, 1, 2, \ldots$). On the other hand, an interesting *real* feature is the maximum at the beginning of the "10" tail ($E \approx 10$ meV). It is due to the fact that excitonic dispersion for $n_e \neq n_h$ is nonmonotonic at small wavevectors q (the ground state occurs at $q > 0$, leading to $dE/dq = 0$ and $d\Gamma/dq \propto q > 0$, i.e., to a singularity in $d\Gamma/dE$).

The curves for $2e+h$ are also dominated by the noninteracting peaks "$n_e n'_e n_h$" corresponding to three unbound particles confined to different combinations of LLs. Low-energy tails describe the exciton with an additional unbound electron, (note oscillations due to excitonic size quantization). Bound trion states appear as discrete peaks below the continuous tails, well visible only in the inset, additionally marked with red and blue bars. All three trions: X^-_{s}, X^-_{td}, and X^-_{tb} appear bound (excitonic ground state is marked by a black bar for comparison). However, weak (< 1 meV) binding of X^-_{s}, virtually equal to X^-_{td}, is an artifact of the unrealistic $n \le 1$ restriction.

The emergence of bound trion states below the exciton's continuum is one noticeable difference between the $e+h$ and $2e+h$ DOS. Another significant effect of the exciton–electron interaction is further (compared to one due to excitonic e–h interaction) smearing of the LLs,

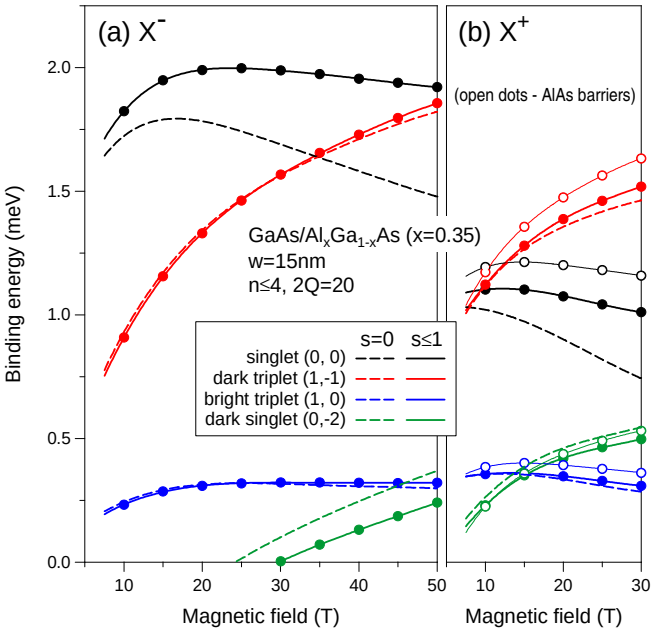

FIG. 2: (color online) Binding energies Δ of four different negative (a) and positive (b) trions $X^\pm$ (the pair of labels in parentheses are two-electron spin S and total angular momentum M) in a symmetric GaAs quantum well of width $w = 15$ nm as a function of magnetic field B, calculated on Haldane sphere with a magnetic monopole strength $2Q = 20$ including five lowest LLs ($n \le 4$) and either one ($s = 0$) or two lowest subbands ($s \le 1$) for each electron and hole. Continuous curves were obtained by interpolation from exact-diagonalization at the values of B marked with dots.

i.e., transfer of the density of states away from LLs and filling the gaps between them. Also, DOS within the inter-LL regions shows features related to the interactions in a nontrivial manner. For example, spin dependence of structures at $E \approx 5$ meV and $E \approx 25$ meV reveals their connection with the (obviously, spin-sensitive) exciton–electron interaction. Note that the $e+h$ peak at $E \approx 10$ meV, identified earlier with an inter-LL exciton, persists in the $2e+h$ curves regardless of spin configuration (to confirm its *one*-electron nature).

The $n \le 1$ restriction to only two lowest LLs was helpful in demonstrating LL smearing and emergence of additional peaks between LLs due to e–h and X–e interactions used in Figs. 1 and 2. However, it gives incorrect exciton and trion energies and, more importantly, ignores the contribution to DOS coming from the neglected higher hole LLs (recall that hole's $\hbar\omega_c$ is only 3.7 meV at $B = 10$ T, much smaller than electron's 17.8 meV).

More accurate trion binding energies (for both X^- and X^+) are plotted in Fig. 2 as a function of B. These values were obtained by including five LLs ($n \le 4$) and up to two subbands ($s \le 1$) for each electron and hole. The lowest-subband ($s = 0$) calculation is similar to Ref. 30, but it used more accurate Coulomb matrix elements, calculated for the actual $\chi_0(z)$. For X^-, an additional,

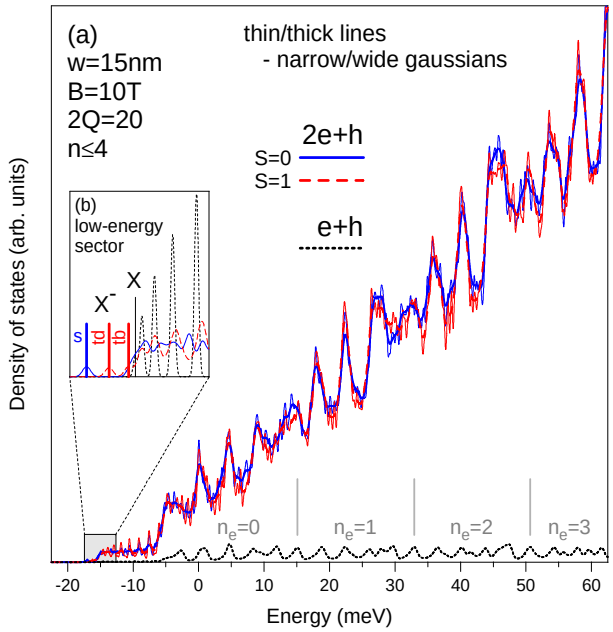

FIG. 3: (color online) The same as in Fig. 1 but for $2Q = 20$, $n \leq 4$, and without dividing $2e + h$ DOS by $g = 2Q + 1$.

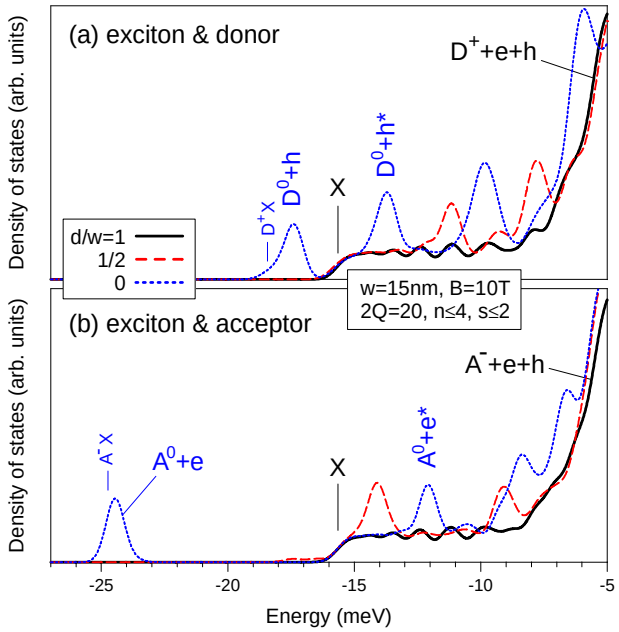

FIG. 4: (color online) Density of states (DOS) of $e + h$ in a symmetric GaAs quantum well of width $w = 15$ nm at magnetic field $B = 10$ T, in the presence of a positive (a) and negative (b) impurity at different distances d from the center of the well, calculated on Haldane sphere with magnetic monopole strength $2Q = 20$ including five LLs ($n \leq 4$) and three subbands ($s \leq 2$) for electron and hole. Continuous curves were obtained by gaussian broadening. Marked bound states: $D^0 = D^+ + e$, $D^+X = D^+ + X$, $A^0 = A^- + h$, and $A^-X = A^- + X$; e^* and h^* denote electron and hole in the excited ($n = 1$) LL.

weakly bound "dark singlet" state occurs only at quite high fields. The curves for $s \leq 1$ demonstrate that in a narrow symmetric well the subband mixing is most efficient for the $M = 0$ singlet, while the lowest-subband approximation is accurate for both triplets.

In our calculations we assumed the Al fraction of $x = 0.35$ in the $Al_xGa_{1-x}As$ barriers. This restriction is justified by the fact that the binding energies of X^- are almost insensitive to the increase of Al fraction all the way up to $x = 1$. The only exception is data for X^+ marked with open dots in Fig. 2(b), obtained for pure AlAs barriers. Evidently, the X^+ binding energies depend more strongly on the barrier height, which must be taken into account in a realistic model.

More accurate DOS is shown in Fig. 3, including five LLs ($n \leq 4$) but still only the lowest subband. Since dimension of the Hilbert space quickly grows with $n_{\max}$ and $2Q$, we were forced to use a smaller $2Q = 20$ in this case (for $2e + h$ this yields dimension 58,875 for the $L_z = S_z = 0$ subspace, whose *all* eigenenergies must be calculated to plot DOS). Especially at higher energies, the curves would become very complicated due to an increasing number of overlapping peaks corresponding to different combinations of n_e and n_h – if not only 5, but *all* LLs were included for the hole. By counting electron cyclotron gaps from the lowest LL peak at $E \approx -e^2/2R$, energies corresponding to consecutive n_e's have been marked with gray vertical lines. Comparison of the curves for $e + h$ (here plotted without rescaling by g^{-1}) and $2e + h$ shows that the effect of smearing the LLs and filling the gaps between them due to X–e interaction is only enhanced when more LLs are included. In the inset, the binding energies of all trion peaks are already well converged for $n \leq 4$ (note however that the lowest subband approximation considerably affects especially the singlet state); the exact values are $\Delta = 1.72$, 0.93, and 0.24 meV for X_s^-, X_{td}^-, and X_{tb}^-, respectively.

An ionized impurity can have a similar effect on the $e+h$ DOS to that of an additional electron. This impurity can be either a positive or negative point charge (ionized donor D^+ or ionized acceptor A^-) placed at a distance d away from the center of the quantum well. The effects of D^+ and A^- are not equivalent due to the e–h asymmetry. Two frames of Fig. 4 show how the $e + h$ DOS changes in the presence of D^+ or A^- placed at $d/w = \frac{1}{2}$ and 0 (edge and center of the well). In plotted energy range (up to the first excitonic maximum "00"), the curves for $d/w = 1$ are almost identical to those without an impurity). One or more bound D^+X or A^-X states (analogous to trions) emerge below the excitonic tail, at the position sensitive to d. Being localized (and nondegenerate), they do not contribute to the macroscopic DOS.

When the impurity approaches the well, a strong peak detaches from "00" and moves to the left through the excitonic tail. It corresponds to the (macroscopically degenerate) $D^0 + h$ or $A^0 + e$ configuration with the unbound e–h pair. In our example, it passes the tail's edge

(X ground state) when the impurity is already inside the well, at $d \approx 3$ nm for D^+ and 5.5 nm for A^-. For $d = 0$, especially the A^0 is bound much more strongly than X. Thus, the strongest effect of an impurity is that, depending on d, it can bring down macroscopic DOS corresponding to unbound e–h below the free excitonic ground state. Certainly, the localized D^+X and A^-X states involving the e–h binding still remain the absolute ground states. Here, the qualitative difference caused by the impurity is that DOS raises abruptly from essentially zero at the nondegenerate bound state to the continuum of degenerate unbound states (instead of through an excitonic tail). Especially the marginally bound A^-X is hardly distinguished from the continuum.

For $d = 0$ we have also marked the $D^0 + h^*$ and $A^0 + e^*$ peaks corresponding to the unbound hole or electron in a higher LL, and thus originating from the "01" and "10" peaks without an impurity. These peaks are separated from $D^0 + h$ and $A^0 + e$ by a cyclotron gap; thus, an impurity mixes the LL peak structure with an excitonic tail due to e–h interaction.

B. Oscillator Strength

Let us now turn to the calculation of oscillator strength Ω for the vac $\leftrightarrow e + h$ and $e \leftrightarrow 2e + h$ optical transitions ("$\rightarrow$" for absorption; "$\leftarrow$" for emission). For a pair of initial and final states, e.g., $\psi = e$ and $\phi = 2e + h$, it is calculated from Fermi's golden rule,

$$\Omega_{\psi\phi} = \sum_k \left| \langle\phi| \, c_k^\dagger c_{\bar{k}}^\dagger \, |\psi\rangle \right|^2 . \qquad (3)$$

Here, $k = [\beta, n, m, \sigma]$ and $\bar{k} = [\bar{\beta}, n, -m, -\sigma]$, and the summation runs over all electron states k in the conduction band and all corresponding hole states $\bar{k}$ in the valence band. Note that according to convention of Eq. (1), $c_k^\dagger$ creates electrons or holes, depending on band index β, leading to the reversed sign of m and σ in $\bar{k}$. The oscillator strength for the recombination of initial $\phi = e + h$ or $2e + h$ states, in the latter case summed over all final $\psi = e$ states, can be expressed as a function of the initial energy $E = E_\phi$,

$$\Omega(E) = \sum_{\psi\phi} \Omega_{\psi\phi} \, \delta(E_\phi - E), \qquad (4)$$

This is the $e + h$ or $2e + h$ "optical density of states" (ODOS). Alternatively, oscillator strength (if necessary, weighted by the occupation function Θ_ψ for the initial states $\psi = e$) can be expressed as a function of the photon energy $\mathcal{E} = E_\phi - E_\psi$,

$$\Omega(\mathcal{E}) = \sum_{\psi\phi} \Omega_{\psi\phi} \Theta_\psi \, \delta(E_\phi - E_\psi - \mathcal{E}). \qquad (5)$$

This is the $\psi \rightarrow \phi$ absorption spectrum (equivalent to ϕ's ODOS for $\psi =$ vac, but not for $\psi = e$).

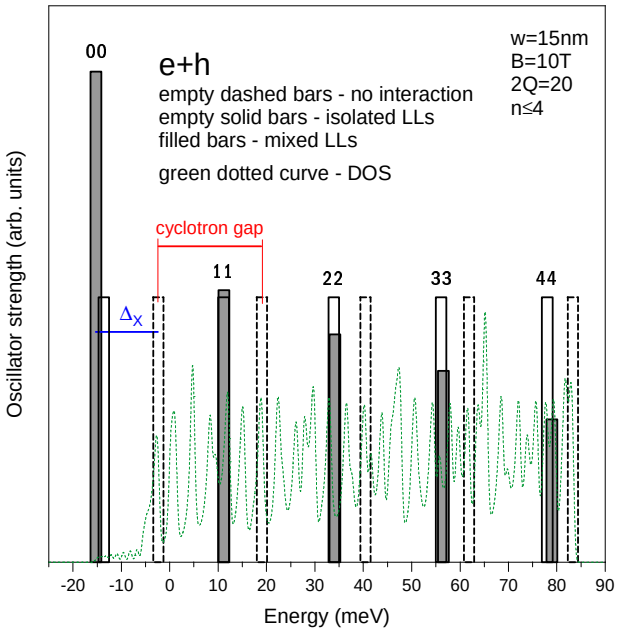

FIG. 5: (color online) Optical density of states (ODOS) of $e + h$, equivalent to absorption spectrum of an exciton, in a symmetric GaAs quantum well of width $w = 15$ nm at magnetic field $B = 10$ T, calculated on Haldane sphere with a magnetic monopole strength $2Q = 20$ including five lowest electron and hole LLs ($n \leq 4$). Results without e–h interaction, with interaction within isolated LLs (peaks marked with LL indices "$n_e n_h$"), and with all interaction effects (including both intra- and inter-LL scattering) are shown. The $e + h$ DOS from Fig. 3 is drawn for reference.

In Fig. 5 we plot ODOS of $e + h$. The parameters ($w = 15$ nm and $B = 10$ T) and Hilbert space ($n \leq 4$ and $2Q = 20$) are the same as in Fig. 3. If the Coulomb energy e^2/λ were much smaller than the cyclotron gaps, then the only optically active states would be the $q = 0$ excitons with electron and hole confined to the same LLs ($n_e = n_h \equiv n$). As shown with empty bars, these excitonic peaks "nn" in $\Omega(\mathcal{E})$ would have equal height and occur at $E(n) = n\hbar(\omega_{c,e} + \omega_{c,h}) - \Delta_X(n)$, where $\Delta_X(n)$ is the exciton binding energy in the nth LL. These energies coincide with the low-energy edges of the excitonic tails of the "nn" peaks in DOS (replotted with a thin dotted line), where degeneracy is absent and DOS vanishes. Since the exciton binding $\Delta_X(n)$ decreases as a function of n, the separation between consecutive peaks also decreases and it is always larger than the cyclotron gap between the corresponding "nn" maxima in DOS. For $w = 15$ and $B = 10$ T, distances between peaks "00", "11", and "22" (calculated excluding LL mixing by setting $v_{ijkl} = 0$ unless $n_i = n_j = n_k = n_l \equiv n$) are $E_{11} - E_{00} = 24.7$ meV and $E_{22} - E_{11} = 22.8$ meV, both considerably larger than $\hbar(\omega_{c,e} + \omega_{c,h}) = 21.5$ meV.

In reality, inter-LL scattering mixes $q = 0$ states with different n. As shown with filled bars, this causes shifting of the peaks (and a further, small increase of the spac-

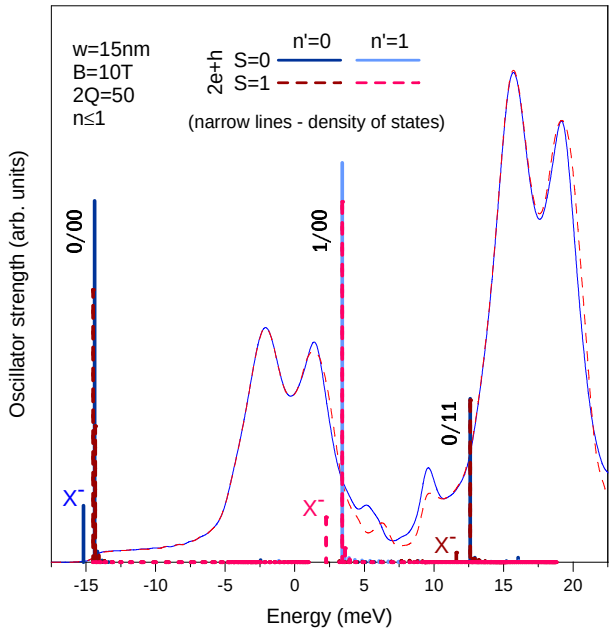

FIG. 6: (color online) Optical density of states (ODOS) of $2e+h$, in a symmetric GaAs quantum well of width $w = 15$ nm at magnetic field $B = 10$ T, calculated on Haldane sphere with a large magnetic monopole strength $2Q = 50$ including only two lowest electron and hole LLs ($n \leq 1$). Singlet and triplet initial $2e + h$ spin configurations ($S = 0$ and 1), and ground and excited final e states ($n' = 0$ and 1) are drawn with different lines. Strongest peaks are marked by LL indices of the initial and final states, "$n'/n_e n_h$" with $n_e = n_h$. Weak peaks associated with bound trions (X^-) are also indicated. The $2e + h$ DOS from Fig. 1 is drawn for reference.

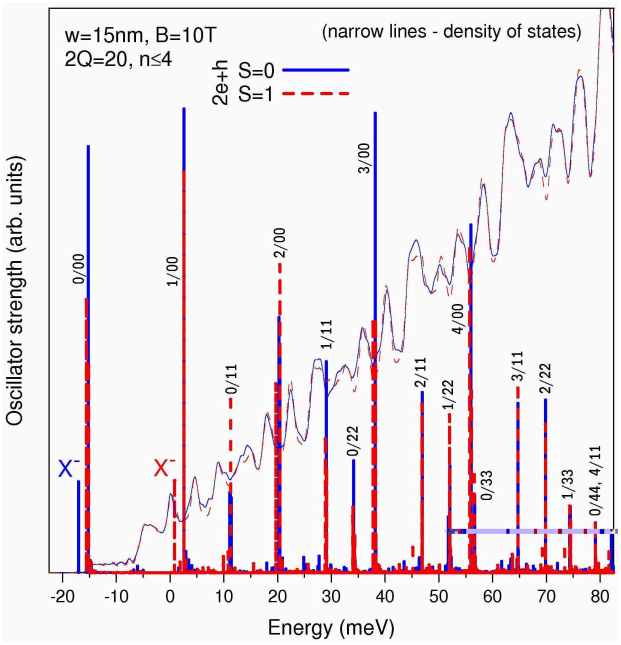

FIG. 7: (color online) The same as in Fig. 6 but for $2Q = 20$ and $n \leq 4$. The strongest peaks are identified as excitonic "n'/nn" transitions or trion recombination (X^-).

ing between neighboring peaks) and transfer of oscillator strength from higher to lower energy. Nevertheless, the effect is perturbative and consecutive peaks can still be labeled by n. For $w = 15$ and $B = 10$ T, the first two gaps in Ω (calculated including all matrix elements v_{ijkl}) increase to $E_{11} - E_{00} = 26.4$ meV and $E_{22} - E_{11} = 23.0$ meV. The relative magnitudes of the lowest three peaks are $\Omega_{11}/\Omega_{00} = 0.55$ and $\Omega_{22}/\Omega_{00} = 0.46$.

In Fig. 6 we plotted ODOS of $2e + h$ calculated using the same Hilbert space ($n \leq 1$ and $2Q = 50$) as in Fig. 1. Also for this larger system there is no apparent correlation between the features in DOS and ODOS. This follows immediately from the $q = 0$ selection rule, equivalent to the requirement of nondegenerate relative motion of the recombining e–h pair, preventing high DOS of a $2e + h$ state involving such a pair.

In analogy to $e + h$, the main peaks can be labeled by "n'/nn", and they correspond to a $q = 0$ exciton created/annihilated on the nth LL, in the presence of the second, ψ-electron on the n'th LL. In those main peaks "n'/nn", the second electron is not bound to the created/annihilated exciton; they describe excitonic optical processes, weakly affected by the exciton–electron scattering. Optically active bound trions (with electrons and holes in different LLs) appear in form of weaker peaks displaced from "n'/nn" by the binding energy. In the lowest LL, the only well resolved trion is the singlet (dark triplet by definition has $\Omega = 0$ and bright triplet is too weakly bound to be distinguished from exciton in this energy scale). In the triplet trion at $E \approx 2.5$ meV one of the electrons is in the $n = 1$ LL. Although unstable against inter-LL relaxation, this state can form by capturing a "00" photo-exciton by a thermally excited electron.

Note that "shake-up" transitions[49] ($n'/nn \leftrightarrow n''$ with $n' \neq n''$, i.e., combination of "nn" recombination with $n' \leftrightarrow n''$ cyclotron excitation of the second electron) are forbidden[50] for an isolated trion due to invariance under 2D (magnetic) translations. This selection rule does not preclude replicas of an exciton and an *unbound* second electron, but these transitions have negligible intensity for $\nu \sim g^{-1} \ll 1$ and cannot be identified in Fig. 6.

Fig. 7 is similar to Fig. 6, but it shows $2e + h$ ODOS calculated with 5 LLs taken into account ($n \leq 4$ and $2Q = 20$). The picture becomes fairly complicated, but the idea is the same. Dominant peaks correspond to excitonic transitions and can be labeled by "n'/nn" (in the calculated spectrum, the assignment is straightforward due to angular momentum conservation in the optical transition, here causing the $L = Q + n'$ selection rule). A great number of weaker transitions that involve exciton–electron interaction emerge around the excitonic peaks. In particular, bright trions appear below "0/00" and "1/00" (singlet and triplet, respectively).

Fig. 8 presents the $2e + h$ absorption spectra $\Omega(\mathcal{E})$, calculated assuming that an electron in the initial state is either in the lowest LL (ground state) or in a higher,

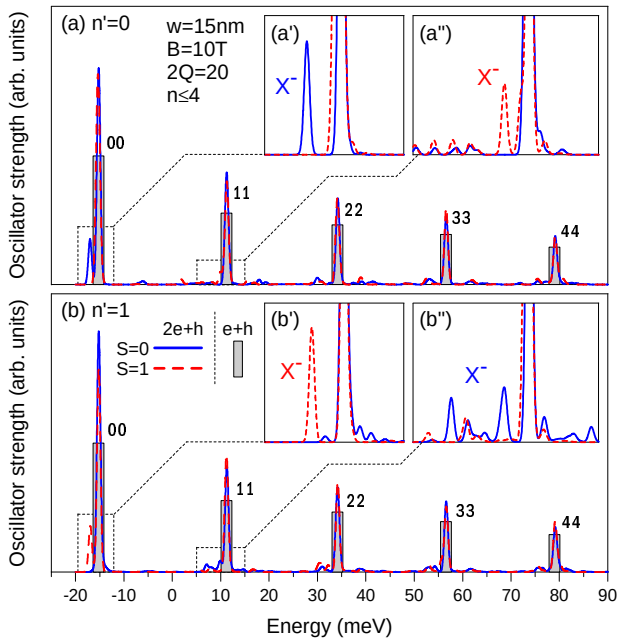

FIG. 8: (color online) $2e + h$ absorption spectra in a symmetric GaAs quantum well of width $w = 15$ nm at magnetic field $B = 10$ T, calculated on Haldane sphere with a magnetic monopole strength $2Q = 20$ including five lowest electron and hole LLs ($n \leq 4$). Continuous curves were obtained by gaussian broadening. Singlet and triplet $2e+h$ spin configurations ($S = 0$ and 1) are drawn separately. Frames (a) and (b) correspond to the initial-state electron in the lowest or first excited LL ($n' = 0$ or 1). The strongest peaks marked as "nn" correspond to excitonic absorption in the nth LL ($e+h$ absorption spectrum from Fig. 5 is shown with gray bars for reference). Insets show magnified regions around the lowest two peaks "00" and "11". Trion peaks (X^-) are identified.

$n = 1$ LL (due to thermal excitation). To observe superposition of many closely spaced small peaks, each discrete $e \to 2e + h$ transition was broadened with a gaussian of width $\delta = 0.5$ meV (main frames) or 0.2 meV (insets). As a reference, the vac $\to e + h$ excitonic spectrum is shown with gray bars.

The main result is that when the (great number of) main ODOS peaks "n'/nn" are shifted by $E_\psi = n'\hbar\omega_{c,e}$ to convert $\Omega(E)$ into $\Omega(\mathcal{E})$, they all fall exactly onto absorption spectrum of a bare exciton. Presence of an additional electron does not cause shifting or splitting of these main absorption lines, and it has insignificant effect on their relative intensities. This demonstrates that, somewhat surprisingly, bare excitonic absorption is unaffected by a dilute electron gas (neither by renormalization of energy nor by transfer of intensity between LLs). This result is obtained for a realistic quantum well, with significant electron–hole asymmetry and LL mixing.

The effect of free electrons is emergence of additional (compared to the bare exciton) features in absorption spectrum, the strongest of them associated with the formation of trions. In Fig. 8, trion absorption peaks can

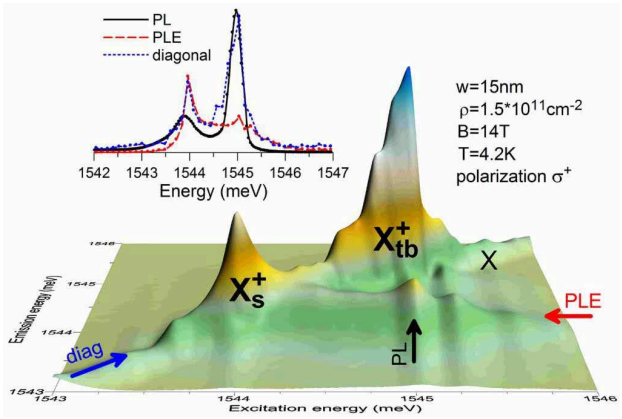

FIG. 9: (color online) Polarized photoluminescence-excitation (PLE) spectrum measured in a symmetric $w = 15$ nm GaAs quantum well with hole concentration $\varrho = 1.5 \cdot 10^{11}$ cm^{-2}, in magnetic field $B = 14$ T, at temperature $T = 4.2$ K.

be seen most clearly in the insets, in which the vicinities of peaks "00" and "11" have been magnified. In reality, their intensity relative to the excitonic peaks will depend on the filling factor and can be much higher than in our model (which represents a very dilute system with only one free electron per $g = 2Q+1$ states of the lowest LL). Remarkably, the spin of strong trion-related features correlates with the parity of $n' - n$: singlet ($S = 0$) peaks appear for $n' = 0$ below "00" and for $n' = 1$ below "11", while triplets ($S = 1$) occur for the opposite combinations of $n' = 0$ with "11" and $n' = 1$ with "00".

IV. EXPERIMENT

To verify some of presented calculations we performed polarization-resolved photoluminescence (PL) and photoluminescence-excitation (PLE) experiments on a symmetric $w = 15$ nm GaAs/AlAs quantum well, containing a valence holes gas with concentration $\varrho = 1.5{\cdot}10^{11}$ cm^{-2} and subject to a strong magnetic field. The PLE experiment consisted of measuring polarization-resolved PL (emission intensity I as a function of emission energy $\mathcal{E}_{\rm out}$) for a series of excitation energies $\mathcal{E}_{\rm in}$. The spectra presented in Fig. 9 were recorded at $T = 4.2$ K, in Faraday configuration, at $B = 14$ T ($\nu \approx 0.45$), and for the circular σ^+ polarization of light (corresponding to optical transitions of an electron in the excited spin state). Emission intensity I is plotted as a function of both $\mathcal{E}_{\rm in}$ and $\mathcal{E}_{\rm out}$. In the inset we showed the following three cross-sections. (i) PL (emission) spectrum is $I(\mathcal{E}_{\rm out})$ for a fixed, high $\mathcal{E}_{\rm in}$. Although it is typically measured for a much higher $\mathcal{E}_{\rm in}$, here we plot the data corresponding to resonant excitation of $X^+_{\rm tb}$. (ii) PLE spectrum is $I(\mathcal{E}_{\rm in})$ for a fixed, low $\mathcal{E}_{\rm out}$, here corresponding to the $X^+_{\rm s}$ recombination. For regular dependence of relaxation on $\mathcal{E}_{\rm in}$, PLE is an indirect measure of absorption. (iii) Diagonal cross-section $I(\mathcal{E}_{\rm out} = \mathcal{E}_{\rm in})$,

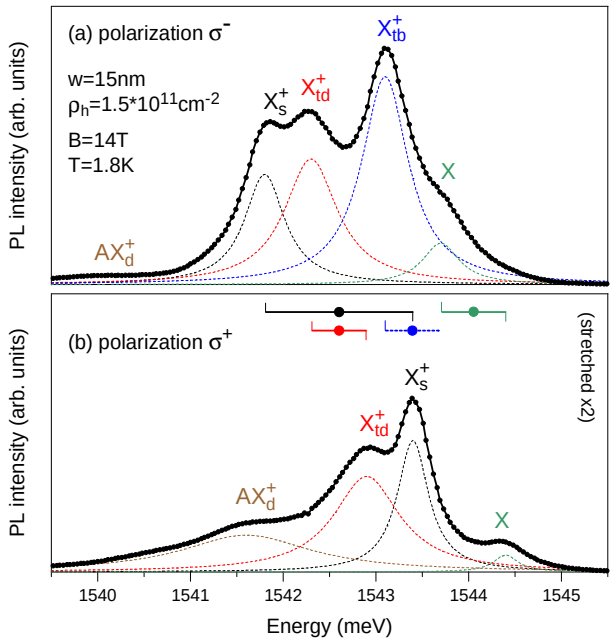

FIG. 10: (color online) Polarized photoluminescence (PL) spectra measured in a symmetric $w = 15$ nm GaAs quantum well with hole concentration $\varrho = 1.5 \cdot 10^{11}$ cm^{-2}, in magnetic field $B = 14$ T, at temperature $T = 1.8$ K.

usually difficult to detect due to strong reflection of the incident light from the surface. By smoothing and appropriate orientation of the surface with respect to the incident/reflected direction we were able to minimize this effect and record meaningful diagonal spectra.

In Fig. 9, two strong peaks correspond to two optically active trions, X_s^+ and X_{tb}^+. Other, minor features are artifacts (note a sizable 0.12 meV step in $\mathcal{E}_{in}$). The suppressed intensity of the X (whose position relative to the X^+'s is anticipated from the following Fig. 10) relative to the bright X^+'s results from a rather large hole concentration. On the other hand, the strongest X_{tb}^+ peak along the diagonal confirms earlier theoretical prediction for the trion oscillator strengths.[30]

In Fig. 10, we plot a pair of polarized σ^- and σ^+ PL spectra $I(\mathcal{E}_{out})$. They were recorded in the same sample and at the same magnetic field as PLE of Fig. 9, but for a higher excitation energy $\mathcal{E}_{in} = 2.57$ eV (wavelength 488 nm) and at low temperature $T = 1.8$ K. Three trion states (X_s^+, X_{td}^+, and X_{tb}^+) along with the exciton are identified for the σ^- polarization. In the σ^+ spectrum, the X_{td}^+ peak is weakened and X_{tb}^+ disappears completely due to spin polarization. Additional low-energy peaks marked as $AX_d^+ = A^0 + X^+$ show recombination of a spin doublet ($S = \frac{1}{2}$) ground state of a trion bound to an neutral acceptor located inside the well (cf. Fig. 4); such impurity-bound trions are discussed elsewhere.[51]

The unambiguous assignment of the peaks was possible from the analysis of the field evolution of the spectra, from $B = 0$ beyond $B = 14$ T, presented in a separate publication.[51] As noted by Glasberg *et al.*,[15] the Zeeman splitting of different X and X^+ states is very different (because of the wavevector dependence of the Landé g-factor for the holes). We marked these splittings with color horizontal bars in Fig. 10(b). The large value of 1.6 meV for X_s^+ (and AX_d^+) compared to only 0.7 meV for X and 0.6 meV for X_{td}^+ is related to the occupation of a strongly repulsive zero-angular-momentum hole pair state, characteristic of the singlet trion (and of doublet AX^+). The analysis of the pair-correlation function shows that this pair state is not occupied also in X_{tb}^+ (despite triplet spin configuration). This lets us expect similar X_{tb}^+ and X_{td}^+ Zeeman splittings, even though X_{tb}^+ is only detected in one polarization.

Knowing the difference between X and X^+ Zeeman splittings is necessary for a meaningful comparison of the trion binding energies Δ with the calculation of Fig. 2(b) in which the Zeeman energy was ignored. The Coulomb binding energies Δ are extracted from the experimental PL spectra by comparing the average X and X^+ energies measured in both polarizations,[15] in Fig. 10(b) marked by dots on the Zeeman bars. In this way, we find $\Delta_s^+ = \Delta_{td}^+ \approx 1.4$ meV and $\Delta_{tb}^+ \approx 0.6$ meV. Compared to these values, the $x = 1$ calculation of Fig. 2(b) predicting $\Delta = 1.2$, 1.35, and 0.4 meV, respectively, slightly underestimates the binding of all three states. The slight discrepancy could result from including only two lowest quantum well subbands and five lowest LLs, assuming equidistant LLs also for the holes, and ignoring the light-hole/heavy-hole mixing, all likely to enhance binding. The numerical tests indicate that neither higher subbands ($s \geq 2$) nor the variation of LL spacing (beyond $n = 1$) play a role, but the the $n \leq 4$ restriction indeed has a noticeable (≤ 0.2 meV) effect on Δ.

The spectra in Fig. 11 are analogous to Fig. 10, but they were recorded on an electron gas and involve negative trions. The sample is also symmetric $w = 15$ nm GaAs quantum well, but the concentration is slightly higher, $\varrho = 2 \cdot 10^{11}$ cm^{-2}, so we had to use a stronger field, $B = 22.5$ T to keep a sufficiently low filling factor, $\nu \approx 0.4$. In both polarizations, the detected trions correspond to those of Fig. 10. The weak X peak marked for σ^- can be identified more convincingly when intensity is plotted in the logarithmic scale. The Zeeman splittings found in this system are 1.8 meV for X_s^- and X_{td}^- (the same value was hence assumed for X_{tb}^-), and 1.4 meV for X. Weaker variation of the splitting supports its attribution to the occupation of two-hole states. Using these splittings, we find the following Coulomb trion binding energies: $\Delta_s^- \approx 2.1$ meV, $\Delta_{td}^- \approx 1.8$ meV, and $\Delta_{tb}^- \approx 0.65$ meV. Again, calculation of Fig. 2(a) predicting $\Delta = 2$, 1.4, and 0.3 meV, respectively, slightly underestimates all these values.

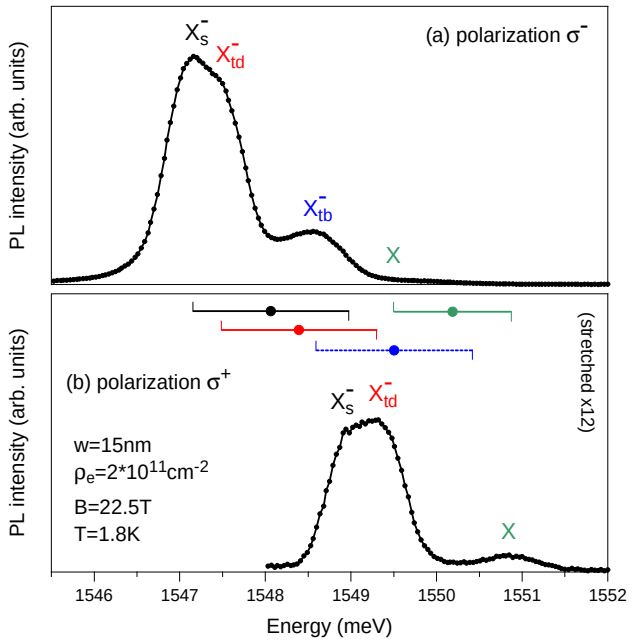

FIG. 11: (color online) Polarized photoluminescence (PL) spectra measured in a symmetric $w = 15$ nm GaAs quantum well with electron concentration $\varrho = 2 \cdot 10^{11}$ cm^{-2}, in magnetic field $B = 22.5$ T, at temperature $T = 1.8$ K.

V. CONCLUSION

We have carried out exact numerical diagonalization of realistic $e+h$ and $2e+h$ hamiltonians (including spin, Coulomb interactions, and mixing of LLs and quantum well subbands) on a Haldane sphere. The parameters used for illustration are adequate for a symmetric 15 nm GaAs quantum well in a magnetic field $B = 10$ T.

Calculation of trion binding energies has been considerably advanced by taking the actual subband wavefunctions for the integration of Coulomb matrix elements and by including five LLs and two quantum well subbands for each electron and hole in the exact diagonalization.

From the full energy spectra we have calculated the density of states (DOS). The main difference between DOS of $e+h$ and $2e+h$, representative for the excitons with and without the presence of additional free electrons, is the emergence of discrete bound trion states below the excitonic tails and redistribution of DOS away from the LL peaks and filling the gaps between them. The effect of an impurity on the $e+h$ DOS is also studied as a function of its charge and position in the well.

For the full spectra of eigenstates, we have calculated the optical oscillator strength Ω. The optical density of states (ODOS) of $2e+h$ shows no obvious correlation with DOS. It is fairly complicated, with a great number of strong transitions labeled by LL indices of the recombining e–h pair and of the left-over electron. However, the $e \to 2e+h$ absorption spectrum is far simpler. It is dominated by a series of LL peaks for the purely excitonic transitions vac $\to e+h$. These main peaks are neither shifted in energy, nor is their intensity noticeably suppressed or enhanced. The presence of (and interaction with) an additional electron shows in form of additional weaker peaks. Some of them are attributed to bound trion states (in the lowest and higher LLs).

The numerical results have been successfully compared with PL/PLE experiments carried out on a 2D hole and electron gases. In particular, absorption and emission of the whole family of both negative and positive trions in the lowest LL has been observed.

Acknowledgments

AW thanks J. J. Quinn for helpful discussions. Work supported by grants: 1P03B03230 and N20210431/0771 (Polish MNiSW), and RITA-CT-2003-505474 (EC).

[1] M. A. Lampert, Phys. Rev. Lett. **1**, 450 (1958).
[2] K. Kheng, R. T. Cox, Y. Merle d'Aubigne, F. Bassani, K. Saminadayar, and S. Tatarenko, Phys. Rev. Lett. **71**, 1752 (1993).
[3] F. Bassani and G. P. Parravicini, *Electronic States and Optical Transitions in Solids* (Pergamon, New York, 1975); E. L. Ivchenko, *Optical Spectroscopy of Semiconductor Nanostructures* (Alpha Science International Ltd., Oxford, 2005); P. Hawrylak and M. Potemski, Phys. Rev. B **56**, 12386 (1997).
[4] G. A. Narvaez, P. Hawrylak, and J. A. Brum, Physica E **9**, 716 (2001).
[5] S. Huant, S. P. Najda, and B. Etienne, Phys. Rev. Lett. **65**, 1486 (1990).
[6] A. B. Dzyubenko, Phys. Rev. B **65** 035318 (2002).
[7] B. Stebe and A. Ainane, Superlatt. Microstruct. **5**, 545 (1989).
[8] H. Buhmann, L. Mansouri, J. Wang, P. H. Beton, N. Mori, L. Eaves, M. Henini, and M. Potemski, Phys. Rev. B **51**, 7969 (1995).
[9] G. Finkelstein, H. Shtrikman, and I. Bar-Joseph, Phys. Rev. Lett. **74**, 976 (1995); Phys. Rev. B **53**, R1709 (1996).
[10] A. J. Shields, M. Pepper, M. Y. Simmons, and D. A. Ritchie, Phys. Rev. B **52**, 7841 (1995).
[11] D. Gekhtman, E. Cohen, A. Ron, and L. N. Pfeiffer, Phys. Rev. B **54**, 10320 (1996).
[12] G. V. Astakhov, D. R. Yakovlev, V. P. Kochereshko, W. Ossau, J. Nürnberger, W. Faschinger, and G. Landwehr, Phys. Rev. B **60**, R8485 (1999); G. V. Astakhov, D. R. Yakovlev, V. P. Kochereshko, W. Ossau, W. Faschinger, J. Puls, F. Henneberger, S. A. Crooker, Q. McCulloch, D. Wolverson, N. A. Gippius, and A. Waag, *ibid.* **65**, 165335 (2002).
[13] O. Homburg, K. Sebald, P. Michler, J. Gutowski, H.

Wenisch, and D. Hommel, Phys. Rev. B **62**, 7413 (2000).
[14] A. J. Shields, J. L. Osborne, M. Y. Simmons, M. Pepper, and D. A. Ritchie, Phys. Rev. B **52**, R5523 (1995).
[15] S. Glasberg, G. Finkelstein, H. Shtrikman, and I. Bar-Joseph, Phys. Rev. B **59**, R10425 (1999).
[16] L. P. Gor'kov and I. E. Dzyaloshinskii, Zh. Eksp. Teor. Fiz. **53**, 717 (1967) [Sov. Phys.—JETP **26**, 449 (1968)].
[17] Yu. A. Bychkov, S. V. Iordanskii, and G. M. Eliashberg, Pis'ma Zh. Eksp. Teor. Fiz. **33**, 152 (1981) [Sov. Phys.—JETP Lett. **33**, 143 (1981)].
[18] C. Kallin and B. I. Halperin, Phys. Rev. B **30**, 5655 (1984).
[19] Y. E. Lozovik, I. V. Ovchinnikov, S. Y. Volkov, L. V. Butov, and D. S. Chemla, Phys. Rev. B **65**, 235304 (2002).
[20] I. Bar-Joseph, Semicond. Sci. Technol. **20**, R29 (2005).
[21] F. M. Peeters, C. Riva, and K. Varga, Physica B **300**, 139 (2001).
[22] A. Wójs and P. Hawrylak, Phys. Rev. B **51**, 10880 (1995).
[23] J. J. Palacios, D. Yoshioka, and A. H. MacDonald, Phys. Rev. B **54**, 2296 (1996).
[24] D. M. Whittaker and A. J. Shields, Phys. Rev. B **56**, 15185 (1997).
[25] M. Hayne, C. L. Jones, R. Bogaerts, C. Riva, A. Usher, F. M. Peeters, F. Herlach, V. V. Moshchalkov, and M. Henini, Phys. Rev. B **59**, 2927 (1999).
[26] F. M. Munteanu, Y. Kim, C. H. Perry, D. G. Rickel, J. A. Simmons, and J. L. Reno, Phys. Rev. B **61**, 4731 (2000); F. M. Munteanu, D. G. Rickel, C. H. Perry, Y. Kim, J. A. Simmons, and J. L. Reno, *ibid.* **62**, 16835 (2000).
[27] G. Yusa, H. Shtrikman, and I. Bar-Joseph, Phys. Rev. Lett. **87**, 216402 (2001).
[28] T. Vanhoucke, M. Hayne, M. Henini, and V. V. Moshchalkov, Phys. Rev. B **63**, 125331 (2001); *ibid.* **65**, 041307 (2002); *ibid.* **65**, 233305 (2002); M. Hayne, T. Vanhoucke, and V. V. Moshchalkov, *ibid.* **68**, 035322 (2003).
[29] G. V. Astakhov, D. R. Yakovlev, V. V. Rudenkov, P. C. M. Christianen, T. Barrick, S. A. Crooker, A. B. Dzyubenko, W. Ossau, J. C. Maan, G. Karczewski, and T. Wojtowicz Phys. Rev. B **71**, 201312 (2005).
[30] A. Wójs, J. J. Quinn, and P. Hawrylak, Phys. Rev. B **62**, 4630 (2000).
[31] C. Riva, F. M. Peeters, and K. Varga, Phys. Rev. B **61**, 13873 (2000); *ibid.* **63**, 115302 (2001); *ibid.* **64**, 235301 (2001).
[32] D. Andronikov, V. Kochereshko, A. Platonov, T. Barrick, S. A. Crooker, and G. Karczewski Phys. Rev. B **72**, 165339 (2005).
[33] J. E. Avron, I. W. Herbst, and B. Simon, Ann. Phys. (N.Y.) **114**, 431 (1978).
[34] A. B. Dzyubenko and A. Y. Sivachenko, Phys. Rev. Lett. **84**, 4429 (2000); A. B. Dzyubenko, Solid State Commun. **113**, 683 (2000).
[35] I. V. Lerner and Yu. E. Lozovik, Zh. Eksp. Teor. Fiz. **80**, 1488 (1981) [Sov. Phys. JETP **53**, 763 (1981)].
[36] A. B. Dzyubenko and Yu. E. Lozovik, Fiz. Tverd. Tela **25**, 1519 (1983) [Sov. Phys. Solid State **25**, 874 (1983)].
[37] A. H. MacDonald and E. H. Rezayi, Phys. Rev. B **42**, 3224 (1990).
[38] C. Schüller, K.-B. Broocks, Ch. Heyn, and D. Heitmann, Phys. Rev. B **65**, 081301 (2002).
[39] C. R. L. P. N. Jeukens, P. C. M. Christianen, J. C. Maan, D. R. Yakovlev, W. Ossau, V. P. Kochereshko, T. Wojtowicz, G. Karczewski, and J. Kossut, Phys. Rev. B **66**, 235318 (2002).
[40] P. Plochocka, P. Kossacki, W. Maslana, J. Cibert, S. Tatarenko, C. Radzewicz, and J. A. Gaj, Phys. Rev. Lett. **92**, 177402 (2004).
[41] B. Stebe, E. Feddi, A. Ainane, and F. Dujardin, Phys. Rev. B **58**, 9926 (1998).
[42] R. B. Laughlin, Phys. Rev. Lett. **50**, 1395 (1983).
[43] A. Wójs, P. Hawrylak, and J. J. Quinn, Phys. Rev. B **60**, 11661 (1999); A. Wójs, I. Szlufarska, K.-S. Yi, and J. J. Quinn, *ibid.* **60**, R11273 (1999).
[44] D. Sanvitto, D. M. Whittaker, A. J. Shields, M. Y. Simmons, D. A. Ritchie, and M. Pepper, Phys. Rev. Lett. **89**, 246805 (2002).
[45] T. T. Wu and C. N. Yang, Nucl. Phys. B **107**, 365 (1976).
[46] F. D. M. Haldane, Phys. Rev. Lett. **51**, 605 (1983).
[47] B. E. Cole, J. M. Chamberlain, M. Henini, T. Cheng, W. Batty, A. Wittlin, J. A. A. J. Perenboom, A. Ardavan, A. Polisski, and J. Singleton, Phys. Rev. B **55**, 2503 (1997).
[48] I.-H. Tan, G. L. Snider, L. D. Chang, and E. L. Hu, J. Appl. Phys. **68**, 4071 (1990).
[49] G. Finkelstein, H. Shtrikman, and I. Bar-Joseph, Phys. Rev. B **53**, 12593 (1996).
[50] A. B. Dzyubenko, Phys. Rev. B **69**, 115332 (2004).
[51] A. Wójs, L. Bryja, J. Misiewicz, M. Potemski, D. Reuter, and A. Wieck, Proc. of XXXV Int. School on Physics of Semicond. Compounds "Jaszowiec 2006," Ustroń, Poland, June 17-23, 2006 (to appear in Acta Phys. Polon. A).